

Elongational Stresses and Cells

Subjects: [Cell Biology](#)

Contributor: Edgar O'Rear

Shear often attributed as being the main source of cell deformation/damage in devices like prosthetic heart valves and artificial organs. Less well understood and studied are extensional stresses which are often found in such devices, in bioreactors, and in normal blood circulation. Several microfluidic channels utilizing hyperbolic, abrupt, or tapered constrictions and cross-flow geometries, have been used to isolate the effects of extensional flow. Under such flow cell deformations, erythrocytes, leukocytes, and a variety of other cell types have been examined. Results suggest that extensional stresses cause larger deformation than shear stresses of the same magnitude. This has further implications in assessing cell injury from mechanical forces in artificial organs and bioreactors. The cells' greater sensitivity to extensional stress has found utility in mechanophenotyping devices, which have been successfully used to identify pathologies that affect cell deformability. Further application outside of biology includes disrupting cells for increased food product stability and harvesting macromolecules for biofuel.

elongational stress

elongational flow

cell mechanics

1. Introduction

Fluid forces and shear stress have become widely appreciated in biology and medicine for their effects on cells. Flow stimulates the release of the potent vasodilator nitric oxide (NO) in the circulatory system ^{[1][2]} and affects anatomy and differentiation in developmental biology ^{[3][4]}. The potential harmful effects of stresses on the cellular and molecular components of blood must be considered when engineers design hemodialysis units and blood-contacting medical devices ^{[5][6][7]}. Both the food and biotechnology industries depend on knowledge of cell mechanics, and the effects of stresses, for optimal processing conditions for products. An appreciation of forces acting on cells is important to understanding many fundamental mechanisms occurring at the cellular scale as well as the response of cells to forces in applied settings.

Shear stress corresponds to just one of the types of forces present during flow. Its mode of action is different than that of an extensional stress. Frictional in nature, shear stresses act at the wall during flow in a tube or blood vessel to oppose the driving force due to pressure. Shear stress or friction also exists between layers of fluid traveling at different velocities in what is called laminar flow, represented in **Figure 1a**. The friction at the wall is such that the fluid layer in immediate contact with the wall has zero velocity. Away from the wall, velocity increases and faster layers apply shear stress on adjacent slower layers in an effort to increase their speed. At the same time, slower layers try to hold the faster layers back with a force opposite to the direction of flow as the effects of friction propagate through the fluid. It has been found experimentally that the very flexible red blood cell (RBC), when placed in a shear stress environment, undergoes an antisymmetric motion called "tank treading", shown in **Figure**

1b [8]. In this case, the cell membrane rotates about the interior of the red blood cell. This is in contrast to other cell types whose rotation in shear flow is more like a solid body. In the circulatory system, shear forces also support leukocyte rolling and adhesion to the endothelium of the vasculature as leukocytes proceed to move out into the tissue to fight infection or contribute to wound healing [9].

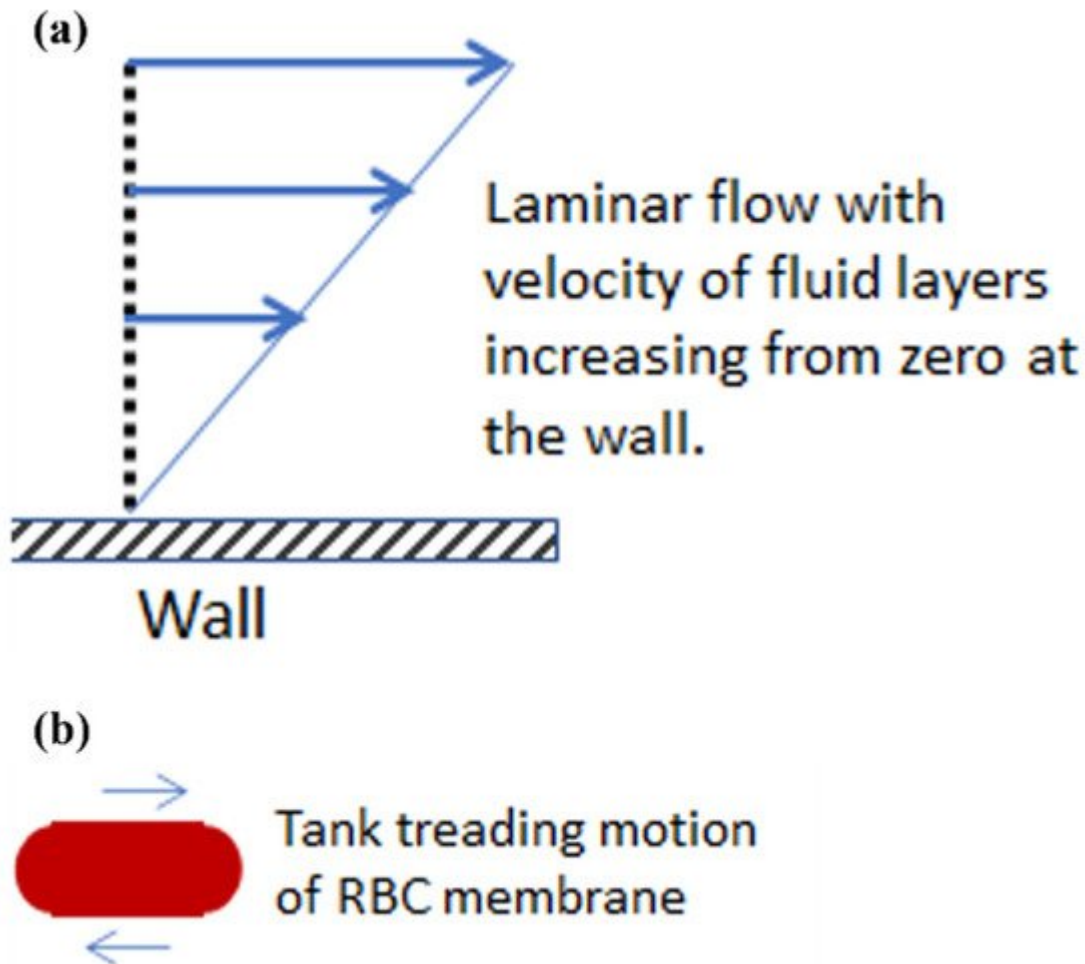


Figure 1. Shear stresses and their effect on red blood cells in laminar flow. (a) Velocity profile of a fluid flowing past a wall in laminar flow. (b) Red blood cell exhibiting a tank treading motion due to shear stresses.

Less well known and understood are the effects of extensional or elongational stresses that are usually present along with shear stresses in many biological flow systems. Typical cases of extensional stresses are found in sudden contractions or expansions of the flow field. For example, many medical devices induce extensional stresses that often remain unaccounted including the entrance and exits of ventricular assist devices, reverse gap flow in artificial heart valves, hypodermic needles, and others [10]. Stresses that are elongational in nature also aid the processing of foods (e.g., tomato concentrates) and biopharmaceuticals (e.g., proteins expressed in *E. coli*) [11] [12]. Considering the prevalence of elongational stresses in many flow systems, it is important to understand how they affect cells and how they compare to shear stresses. In uniaxial elongational flow, a fluid element is stretched at a constant strain rate $\dot{\epsilon}$ so that it narrows (Figure 2a). A constant strain rate means that the distance l between two adjacent points grows at an exponential rate for a simple fluid and, as such, cell exposures to elongational flow

tend to be brief and intermittent due to acceleration of the cell in the flow field. In contrast to the tank tread motion of a red cell undergoing shear, a symmetric stretching of the cell in an extensional flow field does not result in membrane motion (**Figure 2b**). For both shear and elongational stress, however, the aspect ratio of the cell increases until it will not deform further, or the membrane fails. The aspect ratio is defined as the ratio of the length to the width for the projected area of the cell, observed in the video microscopy recordings.

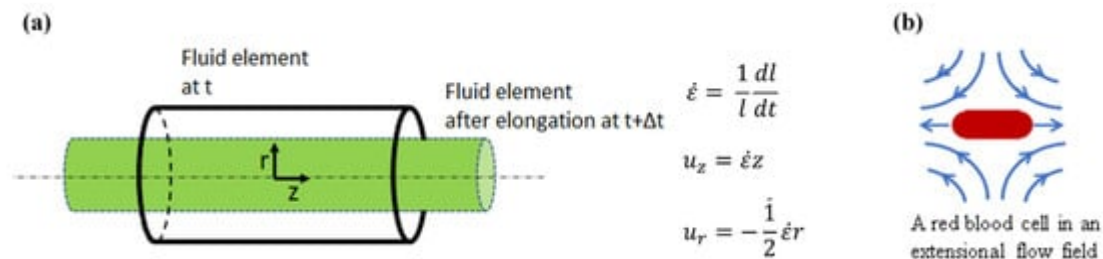


Figure 2. Elongational flow and its effects on red blood cells, as a representative example of cells in general. (a) Uniaxial elongational flow proceeds with a lengthening at the ends and contraction at the center. In a system of set geometry, the elongation rate $\dot{\epsilon}$ at some point in the flow field will increase with applied flow rate. (b) Red blood cell deforming under elongational flow with no membrane rotation.

2. Experimental Methods for Extensional Stresses on Cells

Several well-known methods have been established to examine the effect of shear stresses on cells. These include viscometers used to apply uniform levels of shear stress to suspensions and rectangular microfluidic channels [13][14][15]. Devices used for observing cells under extensional flow also exist with several options for the bioscientist or bioengineer wanting to study the effects of elongational flow on cells, as will be discussed below and summarized in **Table 1**. These fluidic devices typically have a small region where pure extensional flow exists.

Table 1. Summary of experimental methods used for creating elongational flow.

Method	Pros	Cons	Key Results
Hyperbolic Microfluidic Devices	<ul style="list-style-type: none"> Constant elongational rate Magnitude of extensional rate easily controlled High throughput method 	<ul style="list-style-type: none"> Limited region of pure extensional flow Leaking at high flow rates and pressures Trajectory focusing needed 	<ul style="list-style-type: none"> Flow instabilities at high Re and viscoelasticity [16] Achievable extensional stress of 100 Pa [17]

Method	Pros	Cons	Key Results
Abrupt/Tapered Constriction Microfluidic Devices	<ul style="list-style-type: none"> Easily manufactured Magnitude of extensional rate easily controlled High throughput method 	<ul style="list-style-type: none"> Limited region of pure extensional flow Leaking at high flow rates and pressures Trajectory focusing needed 	<ul style="list-style-type: none"> Magnitude of extensional stress higher for abrupt constrictions vs. tapered [10] Flow instabilities at high Re and viscoelasticity Achievable extensional rate of 2000 s^{-1} [18]
Cross-Flow Microfluidic Devices	<ul style="list-style-type: none"> Cells trapped in stagnation point are convenient to observe Bounded flow increases flow stability Magnitude of extensional rate easily controlled 	<ul style="list-style-type: none"> One cell at a time in stagnation zone Not true planar flow Limited region of pure extensional flow Trajectory focusing needed 	<ul style="list-style-type: none"> Flow instabilities at high Re and viscoelasticity Three possible deformation modes [19] Achievable extensional rate of 142 s^{-1} [20]
Optical Tweezers	<ul style="list-style-type: none"> Precise control over applied forces Wide range of forces Longer durations of applied forces 	<ul style="list-style-type: none"> Not a high throughput method Potential of heating cell Expensive equipment 	<ul style="list-style-type: none"> Achievable forces of 600 pN [21]

2.1. Microfluidic Systems Based on Flow through a Contraction

Microfluidic devices utilizing bilaterally symmetric constrictions have been used to create extensional flow regions. In general, flows in microfluidic devices exhibit low Reynolds numbers resulting in laminar flow and parabolic velocity profiles. Away from the center of the parabolic profile shear stresses are present, whereas the middle of the profile is a shear free zone providing a region of pure elongational stresses when flowing through a constriction.

These devices are typically prepared using soft microlithography which places practical limits on the dimensions of the channel, particularly in the depth, and thus on the size of cells suitable for study.

Constrictions following a hyperbolic curve are the ideal option and have been commonly used [16][17][22][23][24][25][26][27]. The basic design of a hyperbolic microfluidic device can be seen in **Figure 3a**, where the hyperbolic curvature of the vessel walls results in the creation of a region of pure extensional flow along the centerline of the channel, free from any shear stress. This unique geometry results in a cross-sectional area that is inversely related to the axial position, which results in a linear increase in velocity along the centerline [16][26]. This linear increase in velocity results in a constant elongational rate along the center line, as expected from the ϵ'_{xx} component of the extensional rate for inviscid flow

$$\epsilon'_{xx} = \delta u_x \delta x \quad (1)$$

and the apparent extensional rate, assuming plug flow (i.e., neglecting any shear flow from the wall), can be estimated according to

$$\epsilon' = QLcd(1/w_d - 1/w_u) \quad (2)$$

where Q is the volumetric flow rate through the channel, w_u and w_d are the initial and final widths of the contraction, respectively, L_c is the length of the contraction, and d is the depth of the channel [16][17][23][26][28]. This equation is strictly only valid when shear effects can be neglected, which is true along the centerline in channel flows. The magnitude of the extension rate is easily controlled, for a given geometry, by adjusting the volumetric flow rate. Ober et al. reported that flow velocimetry measurements of Newtonian fluids show a spatially uniform extension rate as expected, but the value predicted by equation (2) was 66% lower than the true extension rate [16]. They explained that this discrepancy is the result of a 2D approximation of a 3D flow as well as the geometric abruptness of the contraction and the non-rectangular cross-section of the duct due to their fabrication process. To increase the magnitude of the stress in these systems, polymers are often added which increases the viscosity, but may also make the media viscoelastic. Viscoelasticity of the fluid is often denoted by the Deborah number (De), a dimensionless number reflecting the ratio of the elastic forces to the viscous forces or, basically, the relative solid and liquid characters of the material. Higher De numbers signify increased viscoelasticity, which can have significant effects on the flow in the hyperbolic channels. Fluids with low Deborah numbers ($De < O(1)$) behave similar to a Newtonian fluid, as predicted above. For $De > O(1)$ upstream vortices develop that do not affect the spatially homogenous extension rate, while $De > O(10)$ results in a flow that has temporal variations making the determination of the extension rate unreliable [16]. Other limitations to the device are more so related to device construction. Leaking of the channels at high flow rates is not uncommon and limits the achievable maximum extensional rates. In the case of Lee et al., they achieved a maximum rate of 56.2 s^{-1} for a flow rate of $100 \text{ }\mu\text{L}/\text{min}$, achieving a maximum extensional stress of around 3 Pa , while higher flow rates resulted in leaking [23]. Faghieh et al. overcame this limitation and have produced channels withstanding pressures of 350 Pa without leaking, achieving much larger extensional stresses of around 100 Pa [17]. One last limitation is the need to focus the trajectories of particles of interest into the area of pure extensional flow. Cells that are away from the centerline experience levels of shear stress that increase as they get closer to the channel walls. Piergiovanni et al. sought to address this by constructing their microfluidic device with two side channels that delivered sheath fluid to focus

their cells along the centerline [26], while Faghii et al. chose to limit observations to a region in a central band of 20 μm [17]. When it comes to measuring cellular deformation, cell focusing increases the cells found near the centerline of the channel and thereby increases the number of observable cells over a given time period. Focusing the cells along the centerline would be more important when attempting to quantify the presence or absence of cell markers such as lactate dehydrogenase (LDH) release. The lack of trajectory focusing would cause contribution of shear stresses to the response.

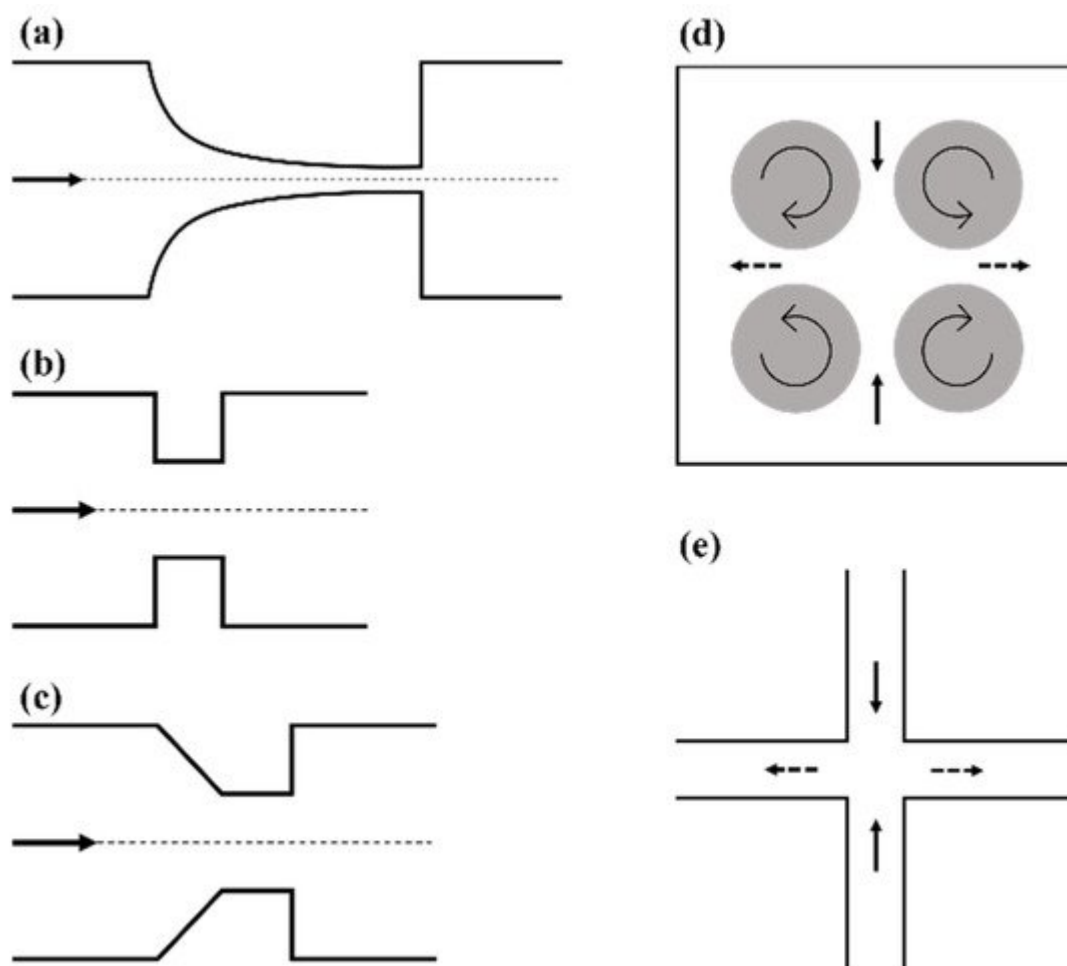


Figure 3. Representative schematics of various extensional flow devices. (a) Hyperbolic converging channel, (b) abrupt constriction, (c) tapered constriction, (d) Taylor's four-roll mill, and (e) cross-flow channel. All arrows show the direction of flow. In (d,e) solid arrows denote the compressional flow axis and dashed arrows denote the extensional flow axis.

In addition to hyperbolic contractions, abrupt and tapered constrictions have also been used to study extensional flows [10][18][29][30]. Their basic design can be seen in **Figure 3b,c**. As with hyperbolic constrictions, the extensional stresses are only found near and within the contraction region due to the increase in velocity experienced there. Computer simulations for abrupt constrictions show that the extensional flow region begins approximately one orifice diameter before the constriction, and that the maximum extension rate is experienced just before the constriction entrance [29]. Similar to hyperbolic channels, pure extensional flow is only experienced along the

centerline of the channel, due to the zero shear stress there, but unlike in hyperbolic channels the extension rate is not constant. This is due to a non-linear increase in velocity through the contraction, thereby resulting in a non-constant extension rate, as seen in Equation (2). Computational fluid dynamics (CFD) analysis of both abrupt and tapered constrictions by Yen et al. showed that the maximum extensional stresses were found at the corners of both types of contractions and that this was also an area of high shear stress as expected [10]. As previously mentioned, there is a region of pure extensional flow along the centerline of the contraction, but the magnitude is smaller than that experienced at the corners [10]. CFD also showed that abrupt contractions result in larger extensional stresses than tapered contractions [10]. Although the extension rate is not constant, it is easily controlled by altering the flow rate, as with the hyperbolic channels. Using a tapered contraction, Mancuso et al. reported a linear increase in maximum extension rate with increasing volumetric flow rate and observed an extension rate of 2000 s^{-1} at a flow rate of $5 \text{ }\mu\text{L}/\text{min}$ [18]. Aside from the non-constant extensional rate and regions of combined extensional and shear stresses, other disadvantages also exist for tapered and abrupt channels. With both, upstream vortices and transient instabilities develop with increasing flow rates and increasing viscoelastic character. As with hyperbolic constrictions, focusing the cells along the centerline would also be beneficial to decrease the effects of shear in bulk measurements as well as increase the number of observable cells in cell deformation studies.

2.2. Taylor's Four-Roll Mill

Seldom used today, Taylor's four-roll mill was one of the earliest reported devices used to create an extensional flow field. The four-roll mill was developed by Taylor to study the breakup of liquid droplets, and was a simple device that created a two dimensional, pure extensional flow [31]. The device as seen in **Figure 3d** is made up of four identical cylinders, each centered such that they sit on the corners of a square, all typically housed in a square box. The cylinders rotate at a given angular velocity with the neighboring cylinders rotating in opposite directions creating two opposed laminar streams. The streamlines of this flow field are rectangular hyperbolas [20][32]. This creates an extensional flow field, with a uniform extension rate, in the center of the area confined by the four cylinders as well as a stagnation point, defined as having zero velocity. Typically, the object of interest would be trapped and observed in the stagnation point where both attractive and repulsive forces are experienced along the compressional and extensional axes, respectively [20]. The extension rate can be predicted using

$$\dot{\epsilon} = 2\pi\Omega\kappa \quad (3)$$

where Ω is the angular speed of the rollers, and κ is a proportionality constant that varies with the fluid medium and design parameters of the mill [20]. Several groups have characterized the flow in the four-roll mill and studied its limitations [32][33][34]. One of the first limitations being the difficulty of maintaining the object of interest in the stagnation point, as reported by Taylor, which can be addressed by adjusting the speed of the left or right pair of cylinders [31]. Additionally, it has been found that with increasing Reynolds numbers, pure extensional flow becomes unstable, developing counter rotating vortices aligned in the stretching direction [34] and a loss of symmetry in the flow pattern [33]. Flows below the critical Reynolds number ($Re_{y,cr} \sim 17$) are stable [34]. The low critical Reynolds number limits the achievable extensional rates in the four-roll mill, not to mention that its size is not suited for examining individual cells. Akbaridoust et al. did construct a functioning miniature four-roll mill

suitable for studying cells, but not without difficulties [20]. Their miniature four-roll mill had fluctuations in the stagnant point position up to 50 μm , due to eccentric rotation of the rollers, and was only able to achieve a maximum strain rate of 6 s^{-1} in a 99% glycerol solution. The already small size of the device made it difficult and expensive to address these issues.

2.3. Cross-Flow Microfluidic Systems

Cross-flow microfluidic devices were a natural progression from Taylor's four-roll mill, and resolved the limitations of Akbaridoust's miniature four-roll mill. The cross-slot microchannel, seen in **Figure 3e**, creates a very similar flow field. The device consists of two opposing inlet channels perpendicular to two opposing outlet channels. Fluid is injected into the inlets and can either be withdrawn at a defined rate or simply allowed to exit through the outlets. This bounded flow provides better flow stability allowing higher strain rates to be achieved, providing an advantage over the four-roll mill [35]. The device creates a planar extensional flow similar to Taylor's four-roll mill with a similar velocity field, hyperbolic streamlines, and a stagnation point in the center where pure planar extensional flow is experienced [20][36]. Objects are trapped in the stagnation point for a finite amount of time and experience compression along the inlet axis and extension along the outlet axis as in the four-roll mill [36][37]. The extensional rate at the stagnant point is inversely related to the channel dimensions according to

$$\dot{\epsilon} \approx 2Uw \quad (4)$$

where U is the average flow velocity in the inlet/outlet channels and w is the channel width [35][38]. Theoretically, this device can achieve high extensional rates, easily controlled by adjusting the volumetric flow rates. Akbaridoust et al. achieved strain rates up to 142 s^{-1} in their cross slot microchannel, which was significantly greater than that achieved in their miniature four-roll mill [20]. Similar to the different types of constriction devices discussed above, cross-slot channels only have a small region of pure extensional flow with shear stresses existing to varying degrees outside of this area. Therefore, it is important to determine the area of uniform extension rate, where cell deformation can be observed. The geometries of cross-slot channels are often described by using a dimensionless number (α), where α is the ratio of the channel depth (d) and width (w). Two-dimensional (2D) numerical simulations of a cross-slot channel with an infinite α show that in a radius of $w/16$ from the stagnation point the extension rate changes less than 5% [36]. Flow velocimetry measurements show an even larger radius ($w/4$) of uniform extension rate in channels with an α of 0.53 [39]. Microparticle image velocimetry (micro-PIV) measurements on a channel with $\alpha = 0.1$ showed that a central region of $0.6 w \times 0.6 w$ resulted in an extension rate variation of 2%, as well as stagnation point variations limited to 1 μm [20]. Clearly, the area of uniform extension rate depends on the channel dimensions and on the flow rates. While these 2D simulations are advantageous, it should be kept in mind that the flow is never truly 2D, and the boundaries on the top and bottom of the device will have effects through the depth of the channel, even for larger values of α which do ensure a more uniform extension rate through the z -axis [35]. As with all the devices discussed thus far, at high enough flow rates or with highly viscoelastic fluids, instabilities occur along with asymmetric flow fields. The asymmetric flow field, characterized as a forward bifurcation, was also confirmed by numerical simulations [40]. Lower values of α had a stabilizing effect for these instabilities [35], but this must be balanced with the fact that a larger α better approaches a 2D planar extensional flow field. Another limitation of cross-slot microchannels is that the cell trajectory through

the channel has significant effects on the strain rates experienced and thus the extent of deformation measured. Henon et al. performed numerical simulations of RBCs flowing through cross-slot microchannels and found three deformation modes depending on the entry position [19]. The first occurs in cells flowing along the centerline of the inlets, which experience very little shear stress and upon reaching the center, near the stagnation point, show large deformations along one axis and remain largely symmetrical. Cells in between the centerline and the walls make up the second mode of deformation, experiencing limited levels of shear stress in the channel arms prior to extensional stresses in the center of the channel leading to asymmetric deformations. The last deformation mode occurs for cells traveling near the wall that experience the highest shear in the channel arms as well as additional shear in the area located between the channel center and the corners resulting from boundary effects, this results in highly asymmetrical cell deformation. Limiting observations to cells in the first category or unifying the cell trajectories, providing a more uniform kinematic history, would yield more accurate deformability measurements. Several studies have used inertial or viscoelastic focusing in cross-slot microchannels to achieve limited cell trajectories [37][41][42]. Using inertial flow ($Re \sim 10^{-1}$) to focus cell trajectories the kinematics of the flow field significantly changed compared to an inertia-less field [37]. Under inertial flow, particles decelerated closer to the stagnation point and had dramatically changed streamlines in the flow field [37]. The strain rate gradient gradually increased with increasing Re , thus shrinking the region with uniform pure extensional flow, and at $Re \geq 40$ vortices developed near the curved walls where the channel arms intersected (i.e., the intersection had rounded corners) [37]. Viscoelastic focusing results in an almost identical flow field to the inertia-less Newtonian case, producing similar velocity fields, streamlines, and regions of uniform strain [37]. Although, using a viscoelastic focusing method, one must consider the issues discussed above for highly viscoelastic fluids. Using such cell focusing methods would produce more accurate measurements of cell deformability and more accurate bulk measurements of cellular damage.

2.4. Optical Tweezers

Optical tweezers can also be used to expose cells to forces that would cause similar deformations experienced under elongational flow. The basis of this method is the ability to trap an object, commonly a silica bead, in a laser beam. This is possible because as the photons from the laser pass through the object they undergo a change in momentum exerting a force which pushes the object to the laser's focal point, thus trapping the object [21]. By attaching beads to the surface of cells, the beads can then be trapped in the optical tweezers and moved, thus stretching the cell. This method allows for easy control and manipulation of the forces exerted onto the cell but is limited as only one cell can be manipulated at a time. This method can apply a range of forces from tens to hundreds of pN, with Dao et al. achieving forces as high as 600 pN [21]. Some downsides to this method are the ability to only examine one cell at a time and the possibility of the laser heating the cell. Lim et al. circumvented this by using larger beads so that the laser was not as close in proximity thereby limiting the possibility of heating [43]. Another concern is the price of this type of equipment, especially considering it requires micromanipulation. Overall, this is a useful technique as the applied force is easily controlled and maintained as long as desired, whereas in microfluidic devices the applied extensional stresses are estimated using computational methods and duration of the stress application is not controlled well.

References

1. Korenaga, R.; Ando, J.; Tsuboi, H.; Yang, W.D.; Sakuma, I.; Toyooka, T.; Kamiya, A. Laminar-Flow Stimulates Atp- and Shear Stress-Dependent Nitric-Oxide Production in Cultured Bovine Endothelial-Cells. *Biochem. Biophys. Res. Commun.* 1994, 198, 213–219.
2. Kuchan, M.J.; Frangos, J.A. Role of Calcium and Calmodulin in Flow-Induced Nitric-Oxide Production in Endothelial-Cells. *Am. J. Physiol.* 1994, 266, C628–C636.
3. Poelmann, R.E.; Groot, A.C.G.D.; Hierck, B.P. The development of the heart and microcirculation: Role of shear stress. *Med. Biol. Eng. Comput.* 2008, 46, 479–484.
4. McIntosh, W.H.; Ozturk, M.; Down, L.A.; Papavassiliou, D.V.; O’Rear, E.A. Hemodynamics of the renal artery ostia with implications for their structural development and efficiency of flow. *Biorheology* 2015, 52, 257–268.
5. Fraser, K.H.; Zhang, T.; Taskin, M.E.; Griffith, B.P.; Wu, Z.J. A quantitative comparison of mechanical blood damage parameters in rotary ventricular assist devices: Shear stress, exposure time and hemolysis index. *J. Biomech. Eng.* 2012, 134, 081002.
6. Federici, A.B.; Budde, U.; Castaman, G.; Rand, J.H.; Tiede, A. Current diagnostic and therapeutic approaches to patients with acquired von Willebrand syndrome: A 2013 update. *Semin. Thromb. Hemost.* 2013, 39, 191–201.
7. Heck, M.L.; Yen, A.; Snyder, T.A.; O’Rear, E.A.; Papavassiliou, D.V. Flow-Field Simulations and Hemolysis Estimates for the Food and Drug Administration Critical Path Initiative Centrifugal Blood Pump. *Artif. Organs* 2017, 41, E129–E140.
8. Fischer, T.; Schmidschonbein, H. Tank Tread Motion of Red-Cell Membranes in Viscometric Flow-Behavior of Intracellular and Extracellular Markers (with Film). *Blood Cells* 1977, 3, 351–365.
9. Ley, K.; Laudanna, C.; Cybulsky, M.I.; Nourshargh, S. Getting to the site of inflammation: The leukocyte adhesion cascade updated. *Nat. Rev. Immunol.* 2007, 7, 678–689.
10. Yen, J.H.; Chen, S.F.; Chern, M.K.; Lu, P.C. The effects of extensional stress on red blood cell hemolysis. *Biomed. Eng. Appl. Basis Commun.* 2015, 27, 1550042.
11. Balasundaram, B.; Harrison, S.T.L. Study of physical and biological factors involved in the disruption of *E. coli* by hydrodynamic cavitation. *Biotechnol. Progr.* 2006, 22, 907–913.
12. Kubo, M.T.K.; Augusto, P.E.D.; Cristianini, M. Effect of high pressure homogenization (HPH) on the physical stability of tomato juice. *Food Res. Int.* 2013, 51, 170–179.
13. Simmonds, M.J.; Atac, N.; Baskurt, O.K.; Meiselman, H.J.; Yalcin, O. Erythrocyte deformability responses to intermittent and continuous subhemolytic shear stress. *Biorheology* 2014, 51, 171–185.

14. Ma, N.N.; Koelling, K.W.; Chalmers, J.J. Fabrication and use of a transient contractional flow device to quantify the sensitivity of mammalian and insect cells to hydrodynamic forces. *Biotechnol. Bioeng.* 2002, 80, 428–437.
15. Buerck, J.P.; Burke, D.K.; Schmidtke, D.W.; Snyder, T.A.; Papavassiliou, D.; O’Rear, E.A. A Flow Induced Autoimmune Response and Accelerated Senescence of Red Blood Cells in Cardiovascular Devices. *Sci. Rep.* 2019, 9, 19443.
16. Ober, T.J.; Haward, S.J.; Pipe, C.J.; Soulages, J.; McKinley, G.H. Microfluidic extensional rheometry using a hyperbolic contraction geometry. *Rheol. Acta* 2013, 52, 529–546.
17. Faghih, M.M.; Sharp, M.K. Deformation of human red blood cells in extensional flow through a hyperbolic contraction. *Biomech. Modeling Mechanobiol.* 2020, 19, 251–261.
18. Mancuso, J.E.; Ristenpart, W.D. Stretching of red blood cells at high strain rates. *Phys. Rev. Fluids* 2017, 2.
19. Henon, Y.; Sheard, G.J.; Fouras, A. Erythrocyte deformation in a microfluidic cross-slot channel. *Rsc Adv.* 2014, 4, 36079–36088.
20. Akbaridoust, F.; Philip, J.; Marusic, I. Assessment of a miniature four-roll mill and a cross-slot microchannel for high-strain-rate stagnation point flows. *Meas. Sci. Technol.* 2018, 29, 045302.
21. Dao, M.; Lim, C.T.; Suresh, S. Mechanics of the human red blood cell deformed by optical tweezers. *J. Mech. Phys. Solids* 2003, 51, 2259–2280.
22. Yaginuma, T.; Oliveira, M.S.N.; Lima, R.; Ishikawa, T.; Yamaguchi, T. Human red blood cell behavior under homogeneous extensional flow in a hyperbolic-shaped microchannel. *Biomicrofluidics* 2013, 7, 054110.
23. Lee, S.S.; Yim, Y.; Ahn, K.H.; Lee, S.J. Extensional flow-based assessment of red blood cell deformability using hyperbolic converging microchannel. *Biomed. Microdevices* 2009, 11, 1021–1027.
24. Faustino, V.; Rodrigues, R.O.; Pinho, D.; Costa, E.; Santos-Silva, A.; Miranda, V.; Amaral, J.S.; Lima, R. A Microfluidic Deformability Assessment of Pathological Red Blood Cells Flowing in a Hyperbolic Converging Microchannel. *Micromachines* 2019, 10, 645.
25. Liu, Y.; Zografos, K.; Fidalgo, J.; Duchêne, C.; Quintard, C.; Darnige, T.; Filipe, V.; Huille, S.; Du Roure, O.; Oliveira, M.S.N.; et al. Optimised hyperbolic microchannels for the mechanical characterisation of bio-particles. *Soft Matter* 2020, 16, 9844–9856.
26. Piergiovanni, M.; Galli, V.; Holzner, G.; Stavrakis, S.; DeMello, A.; Dubini, G. Deformation of leukaemia cell lines in hyperbolic microchannels: Investigating the role of shear and extensional components. *Lab Chip* 2020, 20, 2539–2548.

27. Rodrigues, R.O.; Pinho, D.; Faustino, V.; Lima, R. A simple microfluidic device for the deformability assessment of blood cells in a continuous flow. *Biomed. Microdevices* 2015, 17, 1–9.
28. Oliveira, M.S.N.; Alves, M.A.; Pinho, F.T.; McKinley, G.H. Viscous flow through microfabricated hyperbolic contractions. *Exp. Fluids* 2007, 43, 437–451.
29. Gregoriades, N.; Clay, J.; Ma, N.; Koelling, K.; Chalmers, J.J. Cell damage of microcarrier cultures as a function of local energy dissipation created by a rapid extensional flow. *Biotechnol. Bioeng.* 2000, 69, 171–182.
30. Urbanska, M.; Muñoz, H.E.; Shaw Bagnall, J.; Otto, O.; Manalis, S.R.; Di Carlo, D.; Guck, J. A comparison of microfluidic methods for high-throughput cell deformability measurements. *Nat. Methods* 2020, 17, 587–593.
31. Taylor, G.I. The formation of emulsions in definable fields of flow. *Proc. Math. Phys. Eng.* 1934, 146, 0501–0523.
32. Higdon, J.J.L. The kinematics of the four-roll mill. *Phys. Fluids A Fluid Dyn.* 1993, 5, 274–276.
33. Lagnado, R.R.; Leal, L.G. Visualization of three-dimensional flow in a four-roll mill. *Exp. Fluids* 1990, 9, 25–32.
34. Andreotti, B.; Douady, S.; Couder, Y. An experiment on two aspects of the interaction between strain and vorticity. *J. Fluid Mech.* 2001, 444, 151–174.
35. Haward, S.J. Microfluidic extensional rheometry using stagnation point flow. *Biomicrofluidics* 2016, 10, 043401.
36. Dylla-Spears, R.; Townsend, J.E.; Jen-Jacobson, L.; Sohn, L.L.; Muller, S.J. Single-molecule sequence detection via microfluidic planar extensional flow at a stagnation point. *Lab Chip* 2010, 10, 1543.
37. Kim, J.M. Kinematic analyses of a cross-slot microchannel applicable to cell deformability measurement under inertial or viscoelastic flow. *Korean J. Chem. Eng.* 2015, 32, 2406–2411.
38. Coventry, K.D.; Mackley, M.R. Cross-slot extensional flow birefringence observations of polymer melts using a multi-pass rheometer. *J. Rheol.* 2008, 52, 401–415.
39. Pathak, J.A.; Hudson, S.D. Rheo-optics of Equilibrium Polymer Solutions: Wormlike Micelles in Elongational Flow in a Microfluidic Cross-Slot. *Macromolecules* 2006, 39, 8782–8792.
40. Poole, R.J.; Alves, M.A.; Oliveira, P.J. Purely Elastic Flow Asymmetries. *Phys. Rev. Lett.* 2007, 99, 164503.
41. Kim, J.; Kim, J.Y.; Kim, Y.; Lee, S.J.; Kim, J.M. Shape Measurement of Ellipsoidal Particles in a Cross-Slot Microchannel Utilizing Viscoelastic Particle Focusing. *Anal. Chem.* 2017, 89, 8662–

8666.

42. Cha, S.; Shin, T.; Lee, S.S.; Shim, W.; Lee, G.; Lee, S.J.; Kim, Y.; Kim, J.M. Cell Stretching Measurement Utilizing Viscoelastic Particle Focusing. *Anal. Chem.* 2012, 84, 10471–10477.
 43. Lim, C.T.; Dao, M.; Suresh, S.; Sow, C.H.; Chew, K.T. Large deformation of living cells using laser traps. *Acta Mater.* 2004, 52, 1837–1845.
-

Retrieved from <https://encyclopedia.pub/entry/history/show/34963>